Surface Green's Function of a Piezoelectric Half-Space

Vincent Laude, *Member, IEEE*, Carlos F. Jerez-Hanckes, and Sylvain Ballandras

***Abstract*—The computation of the two-dimensional harmonic spatial-domain Green's function at the surface of a piezoelectric half-space is discussed. Starting from the known form of the Green's function expressed in the spectral domain, the singular contributions are isolated and treated separately. It is found that the surface acoustic wave contributions (i.e., poles in the spectral Green's function) give rise to an anisotropic generalization of the Hankel function $H_0^{(2)}$, the spatial Green's function for the scalar two-dimensional wave equation. The asymptotic behavior at infinity and at the origin (for the electrostatic contribution) also are explicitly treated. The remaining nonsingular part of the spectral Green's function is obtained numerically by a combination of fast Fourier transform and quadrature. Illustrations are given in the case of a substrate of Y-cut lithium niobate.**

I. Introduction

Green's functions are extensively used in the numerical simulation of surface acoustic wave (SAW) transduction problems. Usually in SAW problems, the Green's function relates the excitation at the origin in term of stresses and electrical charges to the response at another point of the surface in terms of mechanical displacements and electric potential [1], [2]. For instance, the finite-element method/boundary-element method (FEM/BEM) relies on a spatial-domain Green's function used to account for wave propagation in the substrate but also to describe the electrostatic response of the substrate. Such Green's functions can include the periodicity of the excitation, as in the case of the periodic FEM/BEM [3]–[9], which describes the propagation of waves in an infinite periodic electrode grating. Because of the use of Floquet waves in the periodic case, it turns out that it is the spectral-domain Green's function that is needed. This is not the case of the so-called finite, two-dimensional (2-D) FEM/BEM, in which the full 1-D spatial Green's function is used [10]. Even though the finite FEM/BEM can describe accurately the response of a finite length SAW device, it cannot take into account the transverse dimension, and hence misses important phenomena such as diffraction and wave guiding effects, or more subtle transverse effects such as the generation of spurious surface waves in the region between electrodes and buses [11]. Many approximate models have been proposed to handle transverse and diffraction effects [12]–[17]. However, a rigorous description should encompass all wave generation, propagation and detection phenomena together with electrostatic effects within the quasistatic approximation [18], [19]. The spatial Green's function of the surface of a piezoelectric half-space is in this sense the most elementary yet complete description of 3-D effects.

The computation of the spatial Green's function of the surface of a piezoelectric half-space relies on the Fourier transform of the spectral Green's function. The spectral Green's function is obtained by assuming plane wave propagation with a given wavevector in the plane of the surface, and solving for the wavevector component along the axis entering the substrate. Hence, it inherently includes a complete 3-D description. In this work, we consider the computation of the full 2-D surface Green's function of a piezoelectric half-space. By 2-D we mean that the spatial variables are considered along the surface with the third dimension (orthogonal to the surface) implicitly included. We consider this problem as a necessary step toward the generalization of 2-D FEM/BEM algorithms to 3-D FEM/BEM algorithms. As remarked above, what is basically needed is to compute the 2-D Fourier transform of the spectral surface Green's function of the piezoelectric half-space. However, this is not straightforward as the most interesting features of the problem arise as singularities of the spectral Green's function. For instance, the surface acoustic waves themselves contribute as poles, and bulk acoustic waves contribute less singularly as discontinuities of the first derivative. Furthermore, the asymptotic behaviors at infinity and at the origin also must be treated with care. In particular, the $1/s$ singularity at the origin only appears in the electrostatic part of the problem.

In Section II, we recall how the spectral Green's function can be computed efficiently, and we discuss the form of the different singular contributions. In Section III, we isolate the case of poles (i.e., SAW contributions at infinity in the spatial domain) and show how the well-known 2-D spatial isotropic Green's function is generalized in the case of anisotropy. In Section IV, we briefly discuss the case of asymptotic contributions and give analytic expressions for them. In Section V, we propose an efficient algorithm to obtain the nonsingular part of the Fourier transform and gather up the different contributions that make up the 2-D spatial Green's function.

Manuscript received June 2, 2005; accepted September 13, 2005.

The authors are with the département LPMO of the Institut Franche-Comté Electronique Mécanique Thermique et Optique-ST, Centre National de la Recherche Scientifique UMR 6174, F-25044 Besançon, France (e-mail: vincent.laude@femto-st.fr).

C. F. Jerez-Hanckes is also with the Centre de Mathématiques Appliquées, Centre National de la Recherche Scientifique UMR 7641, Ecole polytechnique, F-91128 Palaiseau, France, and with Temex, Sophia-Antipolis, F-06904, France.

0885–3010/$20.00 © 2006 IEEE

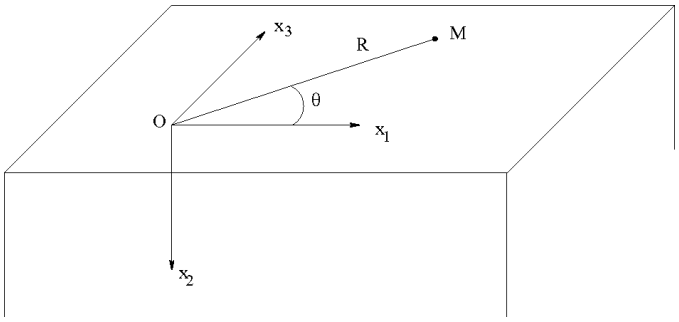

Fig. 1. Definition of axes and coordinates for the computation of the spatial Green's function of a piezoelectric half-space.

II. Spectral Green's Function

The most usual form of the spectral Green's function, or spectral Green's dyadic, for a piezoelectric half-space is in the form of a linear relation between generalized displacements and stresses [20]. The generalized displacements include the mechanical displacements u_1, u_2, u_3, and the electrical potential as $u_4 = \phi$. The generalized stresses include the mechanical stresses applied to the surface T_{21}, T_{22}, T_{23}, and the electrical displacement normal to the surface as $T_{24} = D_2$. Throughout this paper, we assume a time-harmonic dependence of the form $\exp(\imath\omega t)$. The notations for axes are given in Fig. 1. Solving the problem of plane wave propagation with given slownesses s_1 and s_3 along the surface, a linear relation between generalized displacements and stresses is found as:

$$\begin{pmatrix} \tilde{u}_1 \\ \tilde{u}_2 \\ \tilde{u}_3 \\ \tilde{u}_4 \end{pmatrix} = \frac{\tilde{G}(s_1, s_3)}{-\imath\omega} \begin{pmatrix} \tilde{T}_{21} \\ \tilde{T}_{22} \\ \tilde{T}_{23} \\ \tilde{T}_{24} \end{pmatrix}, \tag{1}$$

where we use the tilde over a field (e.g., $\tilde{u}_1$) to emphasize that the quantity is considered in the spectral domain rather than in the spatial domain. In this equation, $\tilde{G}$ is a square matrix of functions of dimension 4, termed the spectral Green's function. Various practical methods for the computation of the spectral Green's function of a piezoelectric half-space have been given in the literature [1], [2], [21], [22]. We assume in the following that $\tilde{G}$ can be obtained efficiently and with great precision.

In this paper, we shall be concerned with obtaining the surface Green's function G in the spatial domain, i.e., the 2-D Fourier transform of $\tilde{G}$. The spatial-domain Green's function of a piezoelectric half-space is here defined as the generalized displacements response to a time-harmonic generalized stress excitation located at the origin. From the spectral Green's function, the spatial Green's function at the point of the surface with polar coordinates (R, θ) is obtained as the 2-D Fourier transform:

$$G(R,\theta) = \int_0^\infty \frac{k\mathrm{d}k}{(2\pi)^2} \int_0^{2\pi} \mathrm{d}\psi \tilde{G}(k,\psi) e^{-\imath kR\cos(\psi-\theta)}. \tag{2}$$

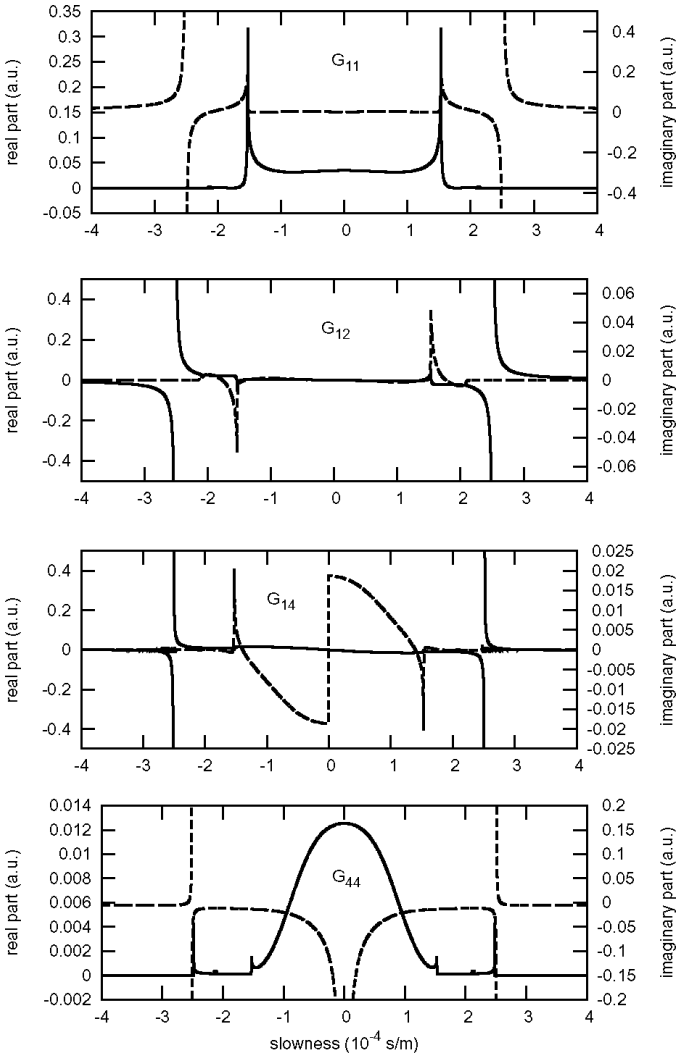

Fig. 2. Cross sections of four of the spectral Green's function components as a function of slowness for Y+128 lithium niobate and X propagation. The real (solid line) and imaginary (dashed line) parts are shown.

This formula follows from the plane wave expansion of the exciting delta function:

$$\begin{aligned} \delta(x_1, x_3) &= \int_{-\infty}^{\infty} \int_{-\infty}^{\infty} \frac{\mathrm{d}k_1 \mathrm{d}k_3}{(2\pi)^2} e^{-\imath(k_1 x_1 + k_3 x_3)} \\ &= \int_0^\infty \frac{k\mathrm{d}k}{(2\pi)^2} \int_0^{2\pi} \mathrm{d}\psi e^{-\imath kR\cos(\psi-\theta)}. \end{aligned} \tag{3}$$

In the above equations, the wave vector $\mathbf{k}$ is linked to the slowness vector $\mathbf{s}$ by $\mathbf{k} = \omega\mathbf{s}$. Furthermore, $k_1 = k\cos(\psi)$ and $k_3 = k\sin(\psi)$.

It is not possible to use directly a numerical algorithm like the fast Fourier transform (FFT) because $\tilde{G}$ has singularities in the spectral plane. Consider the plots in Fig. 2 that display some representative components of $\tilde{G}$ in the particular case of a Y+128 cut lithium niobate half-space as cross sections along the crystallographic X axis. All cross sections exhibit two poles placed symmetrically with

respect to the origin that are the signature of the SAW. We model this pole by a function of the form:

$$\tilde{G}_s(k,\psi) = a_s(\psi)\frac{k_0^2}{k^2 - k_s^2(\psi)}, \tag{4}$$

with $k_s(\psi) = \omega s_s(\psi)$ where $s_s(\psi)$ is the slowness of the SAW in the direction given by ψ obtained on a stress-free surface with open-circuited condition; k_0 is an arbitrarily chosen wave vector used only for normalization purposes; $a_s(\psi)$ amounts for the anisotropy of the electromechanical coupling of the SAW and has the same units as the considered spectral Green's function component. Note that, even though the SAW slowness satisfies the central symmetry property $s(\psi) = s(\psi + \pi)$, such is not necessarily the case for $a_s(\psi)$; $s(\psi)$ and $a_s(\psi)$ can be estimated using fit procedures [15].

There is an additional pole at the origin only in the case of $\tilde{G}_{44}$, i.e., for the electrostatic part of the spectral Green's function only. This pole can be interpreted as arising from the singularity due to an infinite line charge on the surface and is modeled as:

$$\tilde{G}_0(k,\psi) = a_0(\psi)\frac{k_0}{k}. \tag{5}$$

The symmetry relation $a_0(\psi + \pi) = a_0(\psi)$ holds; $a_0(\psi)$ can be obtained as the limit of $k\tilde{G}_{44}/k_0$ as k tends to zero. The asymptotic behavior at infinity for all Green's function components also is governed by a slow $1/k$ decrease that we model as:

$$\tilde{G}_\infty(k,\psi) = a_\infty(\psi)\frac{k_0 k}{k_0^2 + k^2}. \tag{6}$$

This form is chosen such as not to introduce a pole at the origin while still having the required $1/k$ asymptotic behavior at infinity. In the case of $\tilde{G}_{44}$, the value of $a_\infty(\psi)$ includes a correction equal to $-a_0(\psi)$ because (5) introduces a spurious $1/k$ asymptotic behavior at infinity. The symmetry relation $a_\infty(\psi + \pi) = a_\infty(\psi)$ holds; $a_\infty(\psi)$ can be obtained as the limit of $k\tilde{G}_{ij}/k_0$ as k tends to infinity.

A discontinuity at the origin is seen to exist in the case of $\tilde{G}_{14}$. It will be seen later that it is not necessary to model explicitly this form of contribution. Discontinuities of the first derivative of the functions are seen to occur at definite slownesses. These slownesses correspond to bulk acoustic waves propagating in the sagittal plane with their Poynting vector oriented in the direction ψ, the so-called surface skimming bulk waves (SSBW). All these features need to be taken into account in the Fourier transform. Clearly, the surface wave contribution is the most important in the far field in which it is expected to be dominant. Bulk waves are classically expected to decrease faster with increasing distance from the origin of the excitation [1]. It is important to note that, although the discontinuities can be sharp, their dependence with the direction of propagation is always smooth. Fig. 3 displays the slowness curves for the pole created by the SAW and for the bulk acoustic waves within a Y+128 cut lithium niobate half-space.

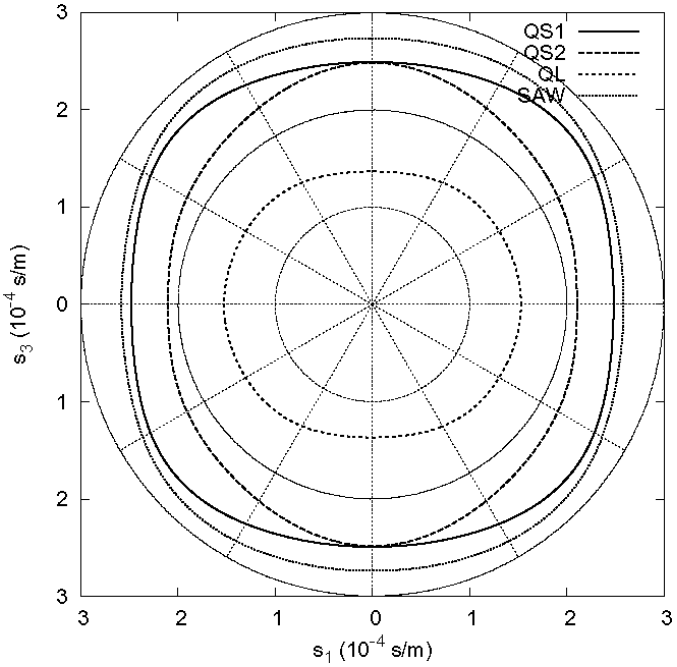

Fig. 3. Slowness curves for the SAW and the bulk acoustic waves (QS1, QS2, QL) propagating in the plane of a Y+128 lithium niobate half-space. QS1 and QS2 stand for the two quasishear bulk acoustic waves, and QL stands for the quasilongitudinal bulk acoustic wave.

The essential features of these slowness curves is that they are very smooth and periodic. These properties will be exploited in the following derivations.

The surface Green's function will be computed by separating the different singular contributions and the regular part of the spectral Green's function. It takes the form:

$$G(R,\theta) = G_s(R,\theta) + G_0(R,\theta) + G_\infty(R,\theta) + G_{ns}(R,\theta), \tag{7}$$

where G_s, G_0, G_∞, and G_{ns} account for the SAW contribution, the electrostatic contribution, the asymptotic contribution at infinity, and the nonsingular contribution, respectively.

III. Surface Acoustic Wave Contribution

The SAW contribution to the spectral Green's function assumes the form of (4). The spatial contribution to the Green's function is then:

$$\begin{aligned} G_s(R,\theta) =& \frac{k_0^2}{(2\pi)^2}\int_0^{2\pi} a_s(\psi)\mathrm{d}\psi, \\ & \int_0^\infty k\mathrm{d}k\frac{e^{-\imath kR\cos(\psi-\theta)}}{k^2 - k_s^2(\psi)}, \end{aligned} \tag{8}$$

where we explicitly take the k-integral before the ψ-integral. The k-integral is singular, and before it can be evaluated by the residue theorem the poles must be displaced slightly from the real axis. Such a procedure is usual in textbooks dealing with Green's functions of the wave

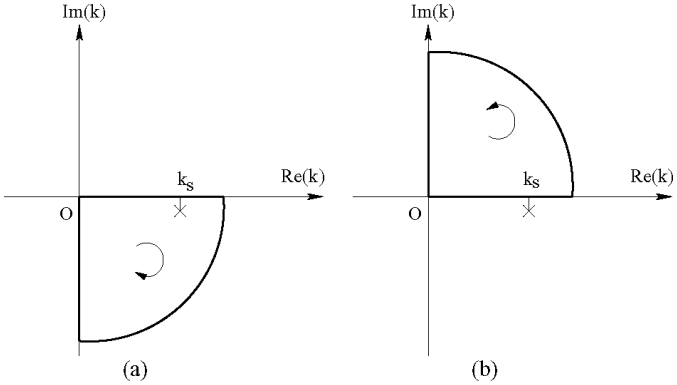

Fig. 4. Contours for integration in the complex k-plane. (a) Contour used when $R\cos(\psi-\theta)>0$. (b) Contour used when $R\cos(\psi-\theta)<0$. The pole k_s due to the SAW is displaced downward vertically from the real axis.

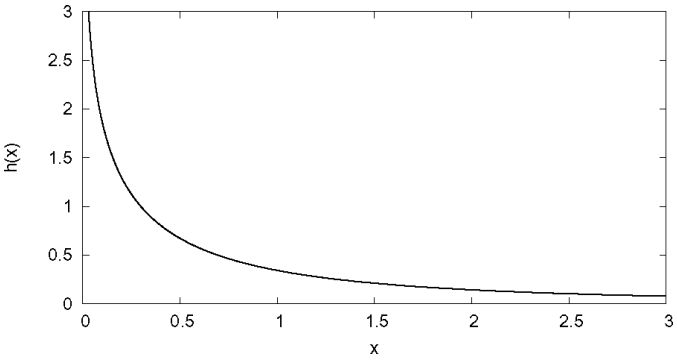

Fig. 5. Plot of function $h(x)$ defined by (10).

equation and can be derived from the principle of limiting absorption [23]. The rule is that the pole at $+k_s(\psi)$ must be displaced downward vertically in the complex plane, and the pole at $-k_s(\psi)$ must be displaced upward vertically. The integration contours in the complex k-plane are indicated in Fig. 4. The result of the integration depends on the sign of $R\cos(\psi-\theta)$. When $R\cos(\psi-\theta)>0$, the integration contour includes the SAW pole and then by application of the residue theorem:

$$\int_0^\infty k\mathrm{d}k\frac{e^{-\imath kR\cos(\psi-\theta)}}{k^2-k_s^2(\psi)}=h(k_s(\psi)R\cos(\psi-\theta)) - \imath\pi\exp(-\imath k_s(\psi)R\cos(\psi-\theta)), \quad (9)$$

with:

$$h(x)=\int_0^\infty y\mathrm{d}y\frac{\exp(-yx)}{y^2+1}. \quad (10)$$

This integral, which has the form of a Laplace transform, is rapidly converging for $x\neq 0$ although divergent at the origin. The function $h(x)$ is easily evaluated numerically by standard algorithms and is plotted in Fig. 5. For small x, $h(x)\approx-\log(x)-\mathcal{C}$ where $\mathcal{C}$ is the Euler constant, and $h(x)\approx 1/x^2$ for large x. When $R\cos(\psi-\theta)<0$, the integration contour does not include the pole and:

$$\int_0^\infty k\mathrm{d}k\frac{e^{-\imath kR\cos(\psi-\theta)}}{k^2-k_s^2(\psi)}=h(k_s(\psi)R|\cos(\psi-\theta)|). \quad (11)$$

Gathering up the results, we obtain that the SAW contribution to the spatial surface Green's function is:

$$G_s(R,\theta)= \frac{k_0^2}{(2\pi)^2}\left(\int_0^{2\pi}\mathrm{d}\phi a_s(\phi+\theta)h(k_s(\phi+\theta)R|\cos\phi| - \imath\pi\int_{-\pi/2}^{\pi/2}\mathrm{d}\phi a_s(\phi+\theta)e^{-\imath k_s(\phi+\theta)R\cos\phi)}\right), \quad (12)$$

with $\phi=\psi-\theta$. This formula generalizes the scalar case as is easily seen by inserting $k_s(\psi)=k_i$ and $a_s(\psi)=a_i$ which, as outlined in the Appendix, results in $G_s(R,\theta)=-\imath(k_0^2a_i/4)H_0^{(2)}(k_iR)$, i.e., that in this case the spatial Green's function is the Hankel function of zero-th order and second kind, as it should [24]. In other words, we have found an integral representation of the SAW contribution to the anisotropic spatial Green's function that generalizes naturally the well-known isotropic case. It is remarkable that the angular integral involves solely the SAW slowness curve, which stresses the intimate relationship between the slowness curve and the far field behavior of waves in anisotropic media. The first integral in (12) is an expansion over evanescent waves that has non-negligible values only in the near field, i.e., close to the origin. The second integral is an expansion over plane waves and is dominant in the far field. Only one-half of the slowness curve is involved in the superposition at the observation point. The involved plane waves can be viewed physically as the only outgoing plane waves emitted at the origin that encounter the observation point.

Fig. 6 displays the SAW contribution to the spatial surface Green's function G_{44} computed for a Y+128 lithium niobate half-space, for three different propagation directions. It can be seen that this function has an oscillatory behavior that resembles that of Bessel functions. In particular, the envelope of the oscillations decreases as $1/\sqrt{R}$ as R increases. The near field disappears rapidly within a few oscillations. It also is seen that the amplitude of the oscillations depends rather strongly on the propagation direction, indicating that the surface Green's function is rather strongly anisotropic. This last point can be emphasized by further observing that the oscillations on the surface concentrate along the wave surface. To see this, the stationary phase principle can be applied to the plane wave expansion in (12) that is dominant in the far field. The stationary points of the integral are given as a function of the observation direction θ by the angles ϕ that satisfy $(\mathrm{d}/\mathrm{d}\phi)(k_s(\phi+\theta)\cos\phi)=0$. This last condition defines the power-flow angle from the slowness surface in anisotropic media.

The case of pseudo or leaky surface waves (LSAW) also is included in the result (12). Indeed, in this case the displacement of the poles from the real axis depicted in Fig. 4 is now not a mathematical artifice but the consequence of the appearance of an imaginary part of the slowness $s_s(\psi)$ [1], [25]–[27].

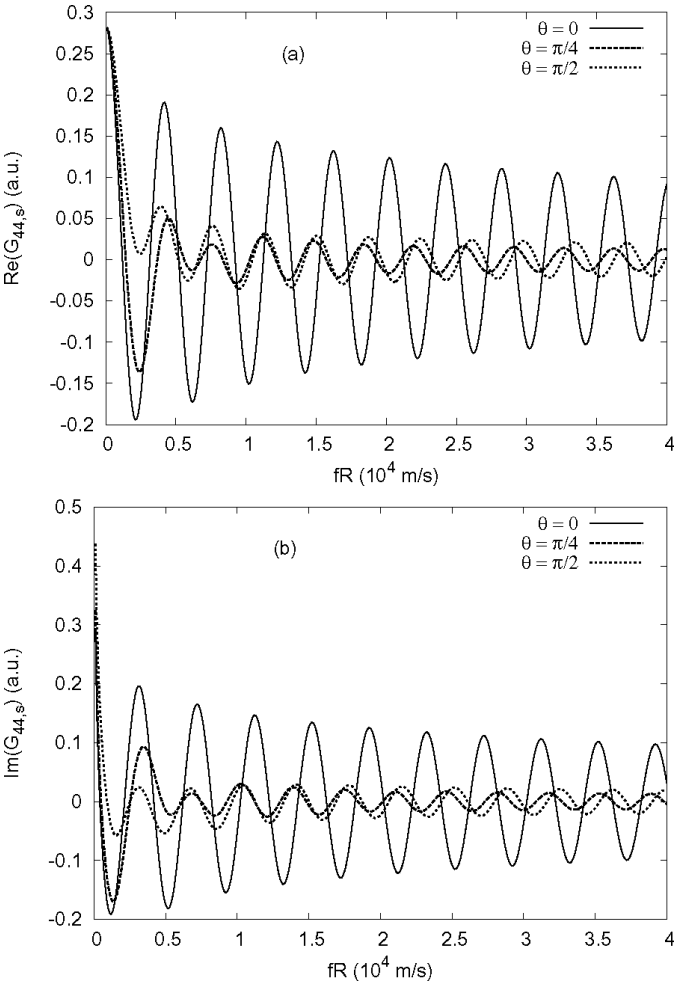

Fig. 6. Real (a) and imaginary (b) parts of $G_{44,s}$, the SAW contribution to the spatial surface Green's function G_{44}, for Y+128 lithium niobate.

IV. Asymptotic Behavior Contribution

As explained in Section II, the asymptotic behavior at the origin of the spectral Green's function is of the form $a_0(\psi)k_0/k$. The asymptotic contribution to the spatial Green's function is then:

$$G_0(R,\theta) = \int_0^\infty \frac{k_0 \mathrm{d}k}{(2\pi)^2} \int_0^{2\pi} \mathrm{d}\phi a_0(\phi+\theta) e^{-\imath kR\cos\phi}. \tag{13}$$

Because a_0 is a 2π-periodic function, we can insert its Fourier series representation:

$$a_0(\psi) = \sum_{n=-\infty}^{\infty} a_{0n} \exp(\imath n\psi), \tag{14}$$

in (13) to obtain:

$$G_0(R,\theta) = \frac{k_0}{2\pi} \sum_{n=-\infty}^{\infty} \imath^n a_{0n} \exp(\imath n\theta) \int_0^\infty J_n(kR)\mathrm{d}k, \tag{15}$$

where the following integral representation of Bessel functions of integer order was used:

$$J_n(x) = \frac{1}{2\pi\imath^n} \int_0^{2\pi} \mathrm{d}y \exp(\imath(ny + x\cos y)). \tag{16}$$

Using the normalization of Bessel function:

$$\int_0^\infty J_n(x)\mathrm{d}x = (\mathrm{sgn}(n))^n, \tag{17}$$

where $\mathrm{sgn}(n)$ is the sign function that equals 1 if $n \geq 0$ and -1 otherwise, we finally have:

$$G_0(R,\theta) = \frac{k_0}{2\pi R} \sum_{n=-\infty}^{\infty} \imath^n (\mathrm{sgn}(n))^n a_{0n} \exp(\imath n\theta). \tag{18}$$

This contribution is easily obtained numerically from the Fourier coefficients of a_0. The $1/R$ behavior at the origin is typical of electrostatic surface problems and the summation accounts for anisotropy.

As explained in Section II, the asymptotic behavior at infinity of the spectral Green's function is of the form $a_\infty(\psi)k_0k/(k_0^2+k^2)$. The asymptotic contribution to the spatial Green's function is then:

$$G_\infty(R,\theta) = \frac{k_0}{(2\pi)^2} \int_0^\infty \frac{k^2}{k_0^2+k^2}\mathrm{d}k \times \int_0^{2\pi} \mathrm{d}\phi a_\infty(\phi+\theta) e^{-\imath kR\cos\phi}. \tag{19}$$

Again, since a_∞ is a 2π-periodic function, we can insert its Fourier series representation:

$$a_\infty(\psi) = \sum_{n=-\infty}^{\infty} a_{\infty n} \exp(\imath n\psi) \tag{20}$$

in (19) to obtain:

$$G_\infty(R,\theta) = \frac{k_0}{2\pi} \sum_{n=-\infty}^{\infty} \imath^n a_{\infty n} e^{\imath n\theta} \int_0^\infty \frac{k^2 J_n(kR)}{k_0^2+k^2}\mathrm{d}k. \tag{21}$$

Using (17), we finally have:

$$G_\infty(R,\theta) = \frac{k_0^2}{2\pi} \sum_{n=-\infty}^{\infty} \imath^n a_{\infty n} \exp(\imath n\theta) \left(\frac{(\mathrm{sgn}(n))^n}{k_0 R} - \int_0^\infty \frac{J_n(yk_0R)}{1+y^2}\mathrm{d}y \right). \tag{22}$$

The integral on the right-hand side of (22) can easily be evaluated by quadrature.

Fig. 7 displays the imaginary part of the asymptotic contributions to the spatial surface Green's function G_{44} for Y+128 lithium niobate half-space, again for three different propagation directions. Note that a_0 and a_∞ are both purely imaginary. It is seen that the asymptotic contributions are mostly localized in the near field and exhibit a $1/R$ dependence at the origin. The anisotropy is very weak in comparison with the SAW amplitude shown in Fig. 6.

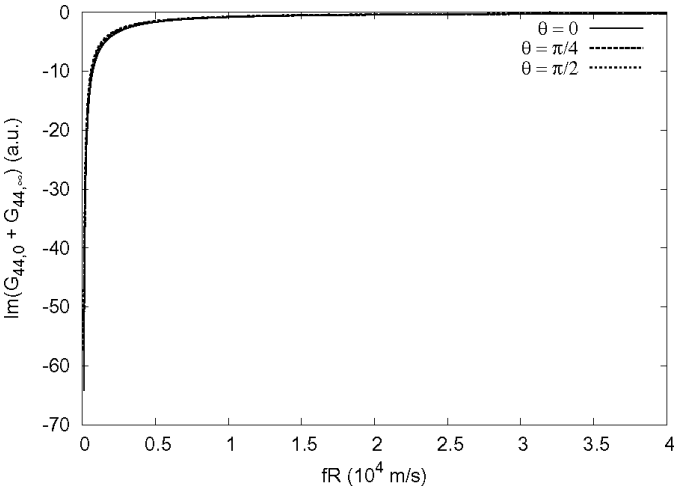

Fig. 7. Imaginary part of $G_{44,0} + G_{44,\infty}$, the asymptotic contributions to the spatial surface Green's function G_{44}, for Y+128 lithium niobate.

V. Nonsingular Part Contribution

The singular contributions discussed above can be efficiently removed from the spectral Green's function by fitting to the models in (4)–(6). The result of this procedure is depicted in Fig. 8 for the three propagation directions already used in plotting Figs. 6 and 7. It can be seen that there remains mostly smooth variations, except at the slownesses of the SSBW in which the derivative can be discontinuous, although the function remains continuous. Only in the direction $\theta = \pi/2$ can a LSAW contribution be seen to remain. This contribution is due to a weak longitudinally polarized LSAW. However, due to its losses, it does not vary too abruptly and the nonsingular spectral Green's function can be sampled at a moderate rate along the slowness axis.

The contribution of the nonsingular part of the spectral Green's function is:

$$G_{ns}(R,\theta) = \int_0^{2\pi} \mathrm{d}\psi \int_0^{\infty} \frac{k\mathrm{d}k}{(2\pi)^2} \times \tilde{G}_{ns}(k,\psi) e^{-\imath kR\cos(\psi-\theta)}. \quad (23)$$

This integral is, of course, nonsingular, but it remains to be evaluated efficiently. A possibility would be to switch back to Cartesian coordinates and take a 2-D FFT of the spectral Green's function. The practical application of this procedure is limited by the sampling requirement along the k-axis. Indeed, $\tilde{G}_{ns}(k,\psi)$ is a relatively fast varying function of k but slowly varying function of ψ. Using Cartesian coordinates means that the sampling along both axes k_1 and k_3 must be as fine as it would be along the radial k axis. Instead, we prefer to use a 1-D FFT along k and a simple quadrature formula along ψ. More precisely we transform (23) to:

$$G_{ns}(R,\theta) = \int_{-\pi/2}^{\pi/2} \mathrm{d}\psi \int_{-\infty}^{\infty} \frac{|k|\mathrm{d}k}{(2\pi)^2} \times \tilde{G}_{ns}(k,\psi) e^{-\imath kR\cos(\psi-\theta)}, \quad (24)$$

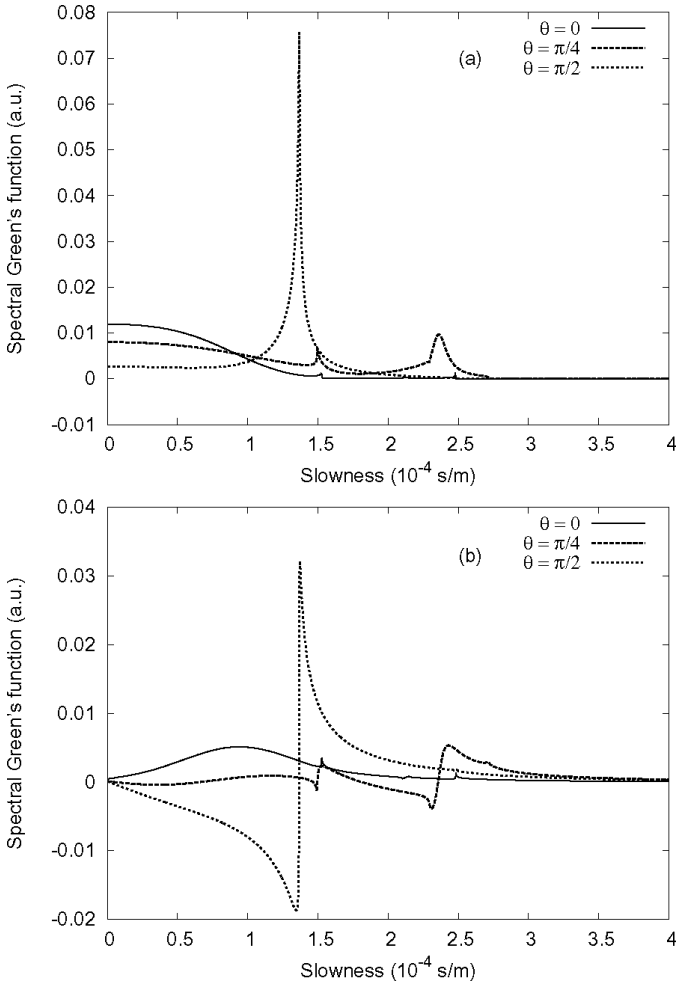

Fig. 8. Real (a) and imaginary (b) parts of the spectral surface Green's function G_{44} with the SAW pole and the asymptotic contributions removed, for Y+128 lithium niobate.

where we extend the domain of definition of the Green's function to negative k-value by the definition $\tilde{G}_{ns}(\psi,-k) = \tilde{G}_{ns}(\psi+\pi,k)$. Noting the Fourier variable $\xi = R\cos(\psi-\theta)$, we obtain:

$$G_{ns}(R,\theta) = \frac{1}{2\pi} \int_{-\pi/2}^{\pi/2} \mathrm{d}\psi \hat{G}_{ns}(\xi,\psi), \quad (25)$$

where $\hat{G}_{ns}(\xi,\psi)$ is the 1-D Fourier transform of $|k|\tilde{G}_{ns}(k,\psi)$ along the k axis. This 1-D Fourier transform is evaluated by FFT for every angle ψ, and the result then is fed back into (24) to evaluate the angular integral. It also can be remarked that discontinuities at the origin as displayed by $\tilde{G}_{14}$ in Fig. 2 are naturally removed by multiplication with $|k|$.

Fig. 9 displays the nonsingular contribution to the spatial surface Green's function G_{44} for Y+128 lithium niobate half-space, again for three different propagation directions. It is mainly concentrated in the near field, with only the longitudinal LSAW giving rise to a pronounced oscillatory behavior for the propagation direction $\theta = \pi/2$. Practically, 16,384 uniformly distributed samples were used along the k-axis for the FFT, and the integration was car-

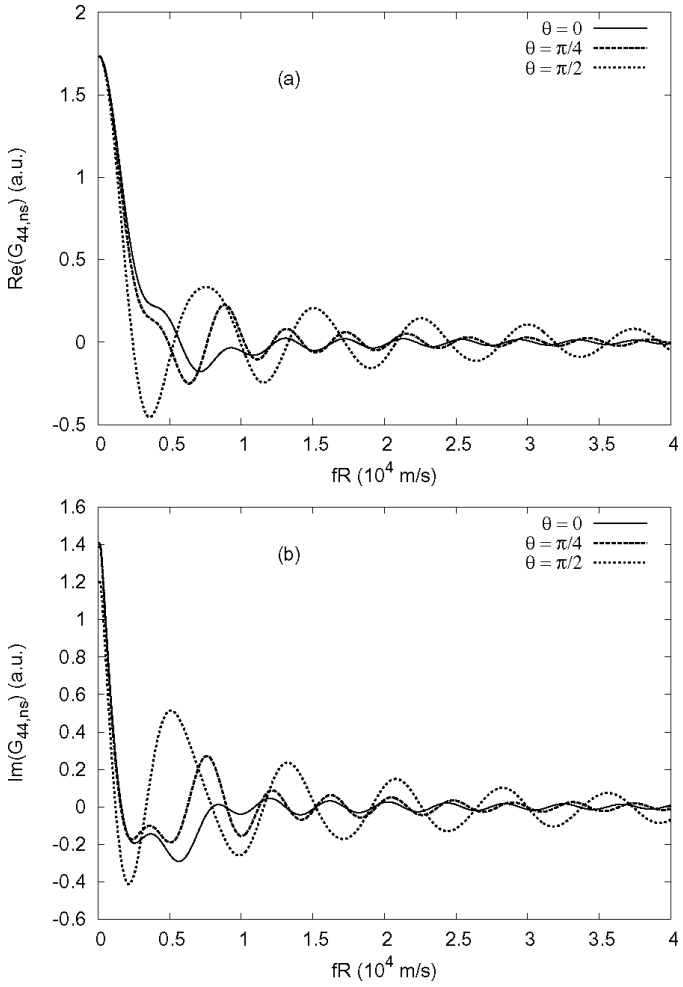

Fig. 9. Real (a) and imaginary (b) parts of $G_{44,ns}$, the nonsingular contribution to the spatial surface Green's function G_{44}, for Y+128 lithium niobate.

ried out from −0.02 to 0.02 s/m in slowness units. The angular integral in (25) was evaluated with one sample per degree and using the trapezoid rule as the quadrature formula. It can be noted that the 1-D FFT can be computed first and stored for each required value of ψ, then be used to obtain the value of $G_{ns}(R,\theta)$ for any observation point in an efficient manner.

Fig. 10 displays the imaginary part of the full surface Green's function of a half-space of Y+128 lithium niobate, i.e., the superposition of the contributions displayed in Figs. 6, 7, and 9.

VI. Conclusions

We have discussed the computation of the 2-D harmonic spatial-domain Green's function at the surface of a piezoelectric half-space. The surface Green's function has been expressed in polar coordinates that are the natural coordinates for a point-source problem. Starting from the known form of the Green's function expressed in the spectral domain, the various singular contributions are isolated and treated separately. It has been demonstrated that the SAW contributions give rise to an anisotropic generalization of the Hankel function $H_0^{(2)}$, the spatial Green's function for the scalar 2-D wave equation. The SAW contributions are dominant in the far field. The asymptotic behavior at infinity and at the origin (for the electrostatic contribution) also have been explicitly treated and shown to affect only the near field. The remaining nonsingular part of the spectral Green's function has been obtained numerically by a combination of FFT along the slowness axis and quadrature over the propagation direction. Illustrations have been given in the case of a Y+128 lithium niobate half-space for the G_{44} Green's function that gives the electrical potential response of the surface to a point charge excitation. The same procedures are straightforwardly extended to purely mechanical or mixed electric-mechanical excitation problems. In addition to its application to the 3-D simulation of SAW devices, we believe that the surface Green's function we have obtained will be useful in the description of SAW in phononic band gap materials [28]–[30].

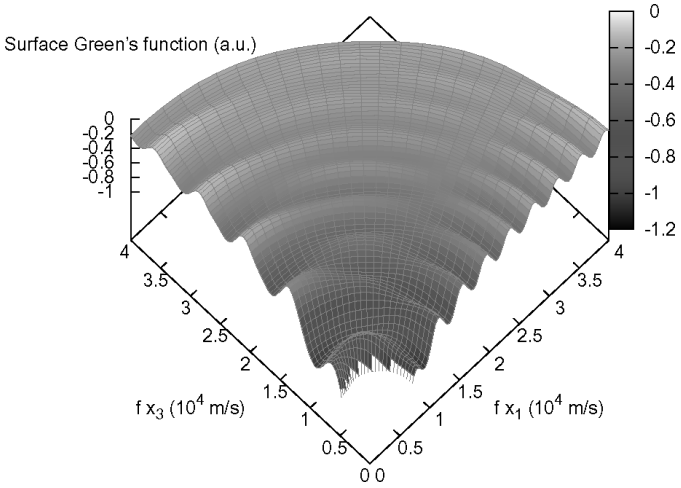

Fig. 10. Imaginary part of the spatial surface Green's function G_{44} for a Y+128 lithium niobate half-space. Only the first quadrant is displayed.

Appendix A

In this appendix, it is shown that the SAW contribution to the spatial Green's function, (12), reduces to $g_s(R,\theta) = -\imath(k_0^2 a_i/4)H_0^{(2)}(k_i R)$ in case of isotropic SAW propagation. Substituting $k_s(\psi) = k_i$ and $a_s(\psi) = a_i$ in (12) we have:

$$G_s(R,\theta) = \frac{k_0^2 a_i}{(2\pi)^2}\left(2\int_{-\pi/2}^{\pi/2} \mathrm{d}\psi h(k_i R\cos\psi) - \imath\pi\int_{-\pi/2}^{\pi/2}\mathrm{d}\psi \exp(-\imath k_i R\cos\psi)\right). \quad (26)$$

Now we have:

$$\begin{aligned}\int_{-\pi/2}^{\pi/2} \mathrm{d}\psi h(k_i R\cos\psi) &= \int_0^\infty \frac{y\mathrm{d}y}{1+y^2}\int_{-\pi/2}^{\pi/2}\mathrm{d}\psi e^{-yk_iR\cos\psi},\\ &= \int_0^\infty e^{-y_1k_iR}\mathrm{d}y_1\int_{-\infty}^{\infty}\frac{\mathrm{d}y_3}{1+y_1^2+y_3^2},\\ &= \int_0^\infty e^{-y_1k_iR}\mathrm{d}y_1\times\frac{\pi}{\sqrt{1+y_1^2}},\\ &= \pi\int_0^\infty \mathrm{d}t\exp(-k_iR\sinh t),\end{aligned} \tag{27}$$

where use has been made of identity 3.111 in [31]. In addition, we have:

$$\int_{-\pi/2}^{\pi/2}\mathrm{d}\psi e^{-\imath k_iR\cos\psi} = \int_0^\pi \mathrm{d}\psi e^{-\imath k_iR\sin\psi}. \tag{28}$$

Remembering the following integral representations of Bessel and Neumann functions (formulas 8.411 and 8.415.4 in [31]):

$$J_0(x) = \frac{1}{\pi}\int_0^\pi \cos(x\sin\theta)\mathrm{d}\theta, \tag{29}$$

$$N_0(x) = \frac{1}{\pi}\int_0^\pi \sin(x\sin\theta)\mathrm{d}\theta - \frac{2}{\pi}\int_0^\infty \mathrm{d}t e^{-x\sinh t}, \tag{30}$$

and the definition of the Hankel function of second kind and zero-th order, $H_0^{(2)}(x) = J_0(x) - \imath N_0(x)$, we finally obtain:

$$g_s(R,\theta) = -\imath(k_0^2a_i/4)H_0^{(2)}(k_iR). \tag{31}$$

References

[1] Y. Zhang, J. Desbois, and L. Boyer, "Characteristic parameters of surface acoustic waves in a periodic metal grating on a piezoelectric substrate," *IEEE Trans. Ultrason., Ferroelect., Freq. Contr.*, vol. 40, no. 3, pp. 183–192, 1993.

[2] R. C. Peach, "A general Green's function analysis for SAW devices," in *Proc. IEEE Ultrason. Symp.*, 1995, pp. 221–225.

[3] H. P. Reichinger and A. R. Baghai-Wadji, "Dynamic 2D analysis of SAW devices including mass-loading," in *Proc. IEEE Ultrason. Symp.*, 1992, pp. 263–266.

[4] H. P. Reichinger, A. R. Baghai-Wadji, and F. J. Seifert, "Stress pattern on the electrode/substrate interfaces in SAW-devices," in *Proc. IEEE Ultrason. Symp.*, 1993, pp. 153–156.

[5] P. Ventura, J. Desbois, and L. Boyer, "A mixed FEM/analytical model of the electrode mechanical perturbation for SAW and PSAW propagation," in *Proc. IEEE Ultrason. Symp.*, 1993, pp. 205–208.

[6] P. Ventura, J. M. Hodé, and M. Solal, "A new efficient combined FEM and periodic Green's function formalism for the analysis of periodic SAW structures," in *Proc. IEEE Ultrason. Symp.*, 1995, pp. 263–269.

[7] G. Endoh, K. Hashimoto, and M. Yamaguchi, "Surface acoustic wave propagation characterization by finite element method and spectral domain analysis," *Jpn. J. Appl. Phys.*, vol. 34, no. 5B, pp. 2638–2641, 1995.

[8] J. Koskela, J. P. Plessky, and M. M. Salomaa, "Suppression of the leaky SAW attenuation with heavy mechanical loading," *IEEE Trans. Ultrason., Ferroelect., Freq. Contr.*, vol. 45, no. 2, pp. 439–449, 1998.

[9] P. Ventura, J.-M. Hodé, J. Desbois, and M. Solal, "Combined FEM and Green's function analysis of periodic SAW structure, application to the calculation of reflection and scattering parameters," *IEEE Trans. Ultrason., Ferroelect., Freq. Contr.*, vol. 48, no. 5, pp. 1259–1274, 2001.

[10] P. Ventura, J. M. Hodé, and B. Lopes, "Rigorous analysis of finite saw devices with arbitrary electrode geometries," in *Proc. IEEE Ultrason. Symp.*, 1995, pp. 257–262.

[11] J. Koskela, J. V. Knuuttila, P. T. Tikka, C. S. Hartmann, V. P. Plessky, and M. M. Salomaa, "Mechanism for acoustic leakage in surface-acoustic wave resonators on rotated y-cut lithium tantalate substrate," *Appl. Phys. Lett.*, vol. 75, no. 17, pp. 2683–2685, 1999.

[12] G. Clark, R. F. Milsom, and J. Schofield, "3-D modal analysis of SAW filters," in *Proc. IEEE Ultrason. Symp.*, 1985, pp. 26–30.

[13] K. Hashimoto, G. Endoh, M. Ohmaru, and M. Yamaguchi, "Analysis of SAWs obliquely propagating under metallic gratings with finite thickness," *Jpn. J. Appl. Phys.*, vol. 35, no. 5B, pp. 3006–3009, 1996.

[14] M. Jungwirth, N. Pocksteiner, G. Kovacs, and R. Weigel, "Analysis of general multi-channel planar waveguides," *IEEE Trans. Ultrason., Ferroelect., Freq. Contr.*, vol. 49, no. 4, pp. 519–527, 2002.

[15] V. Laude and S. Ballandras, "Slowness curves and characteristics of surface acoustic waves propagating obliquely in periodic finite-thickness electrode gratings," *J. Appl. Phys.*, vol. 94, no. 2, pp. 1235–1242, 2003.

[16] M. Solal, "A P-matrix based model for the analysis of SAW transversely coupled resonator filters including guided modes and a continuum of radiated waves," *IEEE Trans. Ultrason., Ferroelect., Freq. Contr.*, vol. 50, no. 12, pp. 1729–1741, 2003.

[17] M. Solal, V. Laude, and S. Ballandras, "A p-matrix based model for SAW grating waveguides taking into account modes conversion at the reflection," *IEEE Trans. Ultrason., Ferroelect., Freq. Contr.*, vol. 51, no. 12, pp. 1690–1696, 2004.

[18] H. Zidek, A. Baghai-Wadji, and F. Seifert, "Full-wave 3D analysis of singly- and doubly-periodic SAW structures," in *Proc. IEEE Ultrason. Symp.*, 1992, pp. 11–14.

[19] H. Zidek, A. Baghai-Wadji, and O. Männer, "Full-wave 3D analysis of wave scattering on SAW-structures with finite aperture," in *Proc. IEEE Ultrason. Symp.*, 1993, pp. 149–152.

[20] A. H. Fahmy and E. L. Adler, "Propagation of surface acoustic waves in multilayers: A matrix description," *Appl. Phys. Lett.*, vol. 22, no. 10, pp. 495–497, 1973.

[21] P. M. Smith, "Dyadic Green]s function for multi-layer SAW substrates," *IEEE Trans. Ultrason., Ferroelect., Freq. Contr.*, vol. 48, no. 1, pp. 171–179, 2001.

[22] T. Pastureaud, V. Laude, and S. Ballandras, "Stable scattering-matrix method for surface acoustic waves in piezoelectric multilayers," *Appl. Phys. Lett.*, vol. 80, no. 14, pp. 2544–2546, 2002.

[23] J. G. Harris, *Linear Elastic Waves*. Cambridge: Cambridge Univ. Press, 2001.

[24] P. M. Morse and H. Feshbach, *Methods of Theoretical Physics*. New York: McGraw-Hill, 1953.

[25] L. Boyer, J. Desbois, Y. Zhang, and J.-M. Hodé, "Theoretical determination of the pseudo surface wave characteristic parameters," in *Proc. IEEE Ultrason. Symp.*, 1991, pp. 354–358.

[26] E. L. Adler, "SAW and pseudo-SAW properties using matrix method," *IEEE Trans. Ultrason., Ferroelect., Freq. Contr.*, vol. 41, no. 6, pp. 876–882, 1994.

[27] V. Laude, M. Wilm, and S. Ballandras, "A least-action principle for the estimation of the slowness and the attenuation of pseudo surface acoustic waves," *J. Appl. Phys.*, vol. 93, no. 12, pp. 10084–10088, 2003.

[28] T. Gorishnyy, C. K. Ullal, M. Maldovan, G. Fytas, and E. L. Thomas, "Hypersonic phononic crystals," *Phys. Rev. Lett.*, vol. 94, p. 115501, 2005.

[29] V. Laude, M. Wilm, S. Benchabane, and A. Khelif, "Full band gap for surface acoustic waves in a piezoelectric phononic crystal," *Phys. Rev. E*, vol. 71, p. 036607, 2005.

[30] T.-T. Wu, L.-C. Wu, and Z.-G. Huang, "Frequency band-gap measurement of two-dimensional air/silicon phononic crystals using layered slanted finger interdigital transducers," *J. Appl. Phys.*, vol. 97, p. 094916, 2005.

[31] I. S. Gradshteyn and I. M. Ryzhik, *Table of Integrals, Series and Products*. 5th ed. New York: Academic, 1994.

Vincent Laude (M'00) was born in Bourg-la-Reine, France, in 1968. He received an Engineering Diploma in 1990 from the Ecole Supérieure d'Optique, and a Ph.D. in Physics in 1994 from Paris XI University, both in Orsay, France. He received his Habilitation à Diriger des Recherches from the Université de Franche-Comté in 2002.

From 1995 to 1999, he was a researcher at Thomson-CSF Corporate Research Laboratory (now Thales TRT) in Orsay, France, where he worked on various aspects of optical signal processing, wavefront sensing, and ultrashort laser pulses. In 2000, he joined Thomson-CSF Microsonics in Sophia-Antipolis, France, to work on surface acoustic wave propagation. At the end of the same year, he joined the Laboratoire de Physique et Métrologie des Oscillateurs, Centre National de la Recherche Scientifique, in Besançon, France. He is currently interested in the propagation of surface, interface, and guided acoustic waves, their interaction with microstructures, phononic band gap materials, and acousto-optics.

Vincent Laude is a member of IEEE/UFFC.

Sylvain Ballandras was born in Strasbourg in 1965. He joined the CNRS in 1991, after receiving his Ph.D. in Engineering Sciences from the Université de Franche-Comté. From 1991 to 1995, he was working on surface acoustic wave (SAW) devices. He was also involved in the development of micromachining technologies (development of LIGA techniques in France, and also micro-stereophotolithography for the manufacture of 3D actuators). In 1995, he oriented his research activities toward industrial and medical applications of ultrasound transducers and also elastic wave guides devoted to signal processing. He has initiated the development of a finite element analysis package devoted to acoustic transducers and also new researches on miniaturized transducers for endoscopic applications. He joined TMX in 1997 for a one year industrial training project. From 1999 to 2005, he was responsible of the research group entitled "Acoustique et Microsonique" at the LPMO. He has created its own consulting office to answer specific demands from industry. In October 2003, he was promoted to Research Director at the CNRS in the newly created FEMTO-ST Institute in Besançon. In June 2005, he left the responsibility of its research group to assume the direction of the joined laboratory between TEMEX and FEMTO-ST devoted to SAW filters and sensors. His main interests concern elastic wave guides for high frequency signal processing and wireless sensors, as well as acoustic imaging transducers for medical and NDE applications.